Twin-Grid Array as 3.6 GHz Epidermal Antenna for Potential Backscattering 5G Communication

Jack D. Hughes, Cecilia Occhiuzzi, John Batchelor, and Gaetano Marrocco

Abstract—Emerging 5G infrastructures can boost innovative paradigms for future wearable and epidermal devices exploiting low-power (even passive) wireless backscattering-based communication. To compensate high body and path losses, and to extend the read range, array configurations are required. This letter proposes a flexible monolithic epidermal layout, based on the Krauss array concept, that operates at 3.6 GHz, and it is suitable to be directly attached to the human body. The antenna involves a dual-grid configuration with a main radiating grid backed by a grid reflector placed in touch with the skin. Overall, the number of conductors and dielectric substrates is minimized with benefit to breathability. The antenna is suitable for surface feeding and produces a broad-side radiation. Parametric analysis is performed, and an optimal configuration of a four-cell grid is derived and experimentally demonstrated to provide a maximum gain of more than 6 dBi.

Index Terms—Epidermal array antenna, epidermal electronics, flexible electronics, 5G antenna.

I. I NTRODUCTION

EPIDERMAL electronics [1] is an emerging research trend aimed at developing medical devices in a soft, flexible, and sometimes stretchable format for direct on-skin application. These devices are often passive, referring to a system without a battery, working on harvested power alone, hence reducing the impact on energy, waste, and pollution while requiring minimal maintenance [2]. The mostly used communication strategy in this regard is backscattering coding, which allows an epidermal node to transmit data by reflecting and modulating an incident RF wave [3]. Nowadays, backscattering communication is widely deployed in the ultrahigh frequency (UHF) band (860–960 MHz) by radio frequency identification (RFID) technology and can be considered a reference platform for epidermal devices [4], thanks to the absence of batteries, the minimal electronics, the sensing capabilities, and the possibility to reach a read distance of up to 1–2 m. Coupling this with currently developing fifth-generation (5G) communication systems makes body-centric communication an unprecedented opportunity for both leisure and medical applications [5]. It is expected that future 5G devices will be able to interact with epidermal devices via batteryless backscattering communications, granting the capability to retrieve multiple biophysical electrical signals or track muscles and body motions in real time and with high accuracy [6]. Preliminary studies have demonstrated that the new 5G frequency within the S-band (3.6 GHz) has advantages over UHF RFID [6] for backscattering links involving epidermal tags. Namely, despite the higher free space attenuation, 3.6 GHz antennas are suitable to provide comparable read distance to on-skin UHF, while boasting smaller layout and much higher data rate.

One-lambda loops are largely recognized as suitable for epidermal antennas [7]. Studies in the UHF and 5G S-bands demonstrated that optimal loop configurations exist [6], [8]. Namely, at 3.6 GHz, a maximum radiation gain of $G_{\max} \approx -5$ dB can be achieved with a single miniaturized 17.5 × 17.5 mm2 loop placed 0.25 mm from the body. To improve gain, mitigate path and body losses, and obtain greater communication distances, multiple antennas in array configuration can be adopted. Preliminary numerical results in [6] investigated the upper bound performances achievable by varying the number of array elements; however, no attempt has been made to engineer and prototype a final layout with the required beam forming network.

Typical array configurations for body-centric communications include patches and slot antennas [9]. At higher frequencies, more directive layouts such as Yagi–Uda or 3-D layouts have also been proposed [10]. However, their structures lack the required flexibility to conform to the body; furthermore, they integrate large conducting ground planes (or electromagnetic bandgap structures [11]), making it difficult for the skin to breathe, also requiring complicated and intricate feed networks for proper functionality. Even if mitigation can be obtained by exploiting textile materials and flexible substrates [12], their application to epidermal electronics is still in question.

Recently, Occhiuzzi and Marrocco [13] have proposed the use of a monolithic epidermal array (layout in Fig. 1) that is based on loop antennas arranged as a Kraus grid [14]. The Kraus grid has found application at millimetre-wave frequency for antenna-in package technology [15], thanks to high gain, bandwidth, simple feed, low profile, lightness, and relatively straightforward construction. However, the presence of the ground plane introduces a challenge for epidermal applications, as it makes the device more rigid and less breathable. A groundless configuration for on-skin applications was, hence, numerically investigated at 60 GHz [13]; since the skin is highly reflective at this frequency, it operates as the ground plane. At 3.6 GHz, the electromagnetic interaction with the body cannot be neglected, and the removal of the ground plane would greatly reduce the radiation efficiency. To overcome this limitation, this letter proposes and experimentally evaluates a new array layout with a twin structure comprising a driver (radiating) grid and a reflector grid. The reflector grid still partially decouples the antenna from the body maintaining the broadside radiation of the Kraus grid, with the benefit of leaving most of the area uncovered by conductors and substrate. To make the device compatible with surface-mounted electronics, the antenna is fed at the middle of the central vertical element through a coplanar impedance transformer.

The rest of this letter is organized as follows. In Section II, the layout of the epidermal grid array is presented, together with a parametric analysis devoted to defining the upper bound performances. A synthesis of a microstrip grid array antenna is then presented in Section III. This letter concludes with prototypes and measurements in realistic conditions.

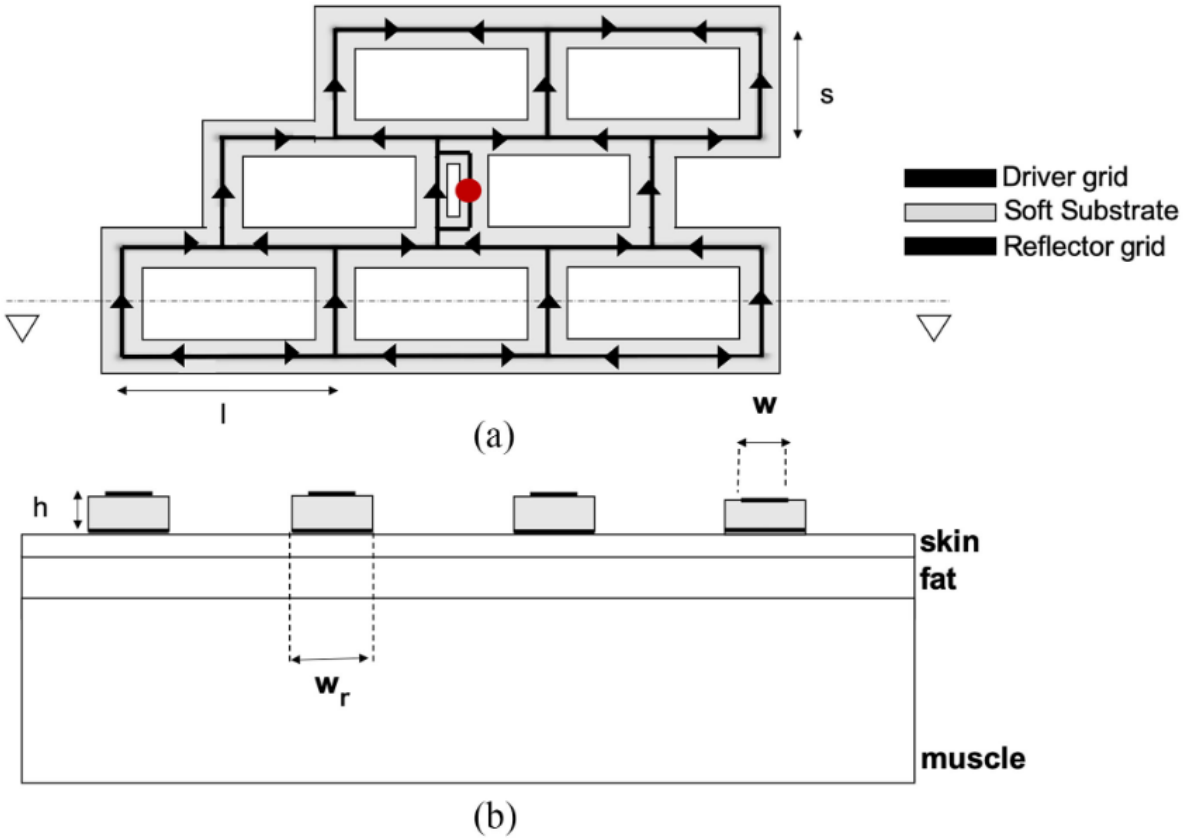

Fig. 1. Schematic representation of the twin-grid antenna array and pattern of currents. Feed is planar and located on the central element through a T-match impedance transformer. (a) Top view. (b) Section with the three-layer numerical body phantom adopted in finite-difference time-domain simulations (CST Microwave Studio).

II. ANTENNA LAYOUT

The proposed twin-grid array has a continuous structure consisting of loop cells with dimensions s ≈ λ_{wg} /2 and l = 2 s, λ_{wg} is the guided wavelength [16] at the centre frequency of operation f0, evaluated under the simplified hypothesis of a continuous (full) ground under the grid and by considering the microstrip width w and the thickness h of the substrate [15], staggered by λ_{wg} /2 between rows as to make the shape shown in Fig. 1. The structure is resonant, the currents on vertical elements are in phase and act as radiators, and couplets of horizontal currents are in phase reversal acting as transmission lines. To partially decouple the antenna from the human body, a twin grid is adopted as a reflector in direct contact with the human skin. Between the grids, a lightweight, flexible, and biocompatible substrate is included (silicone rubber, with permittivity ε_r = 3 and tan δ = 1.4×10^{-3}). Both the substrate and the reflector follow the driver shape, leaving uncovered a large part of the skin surface benefiting the breathability and wearability of the antenna and enabling the possibility to directly access the human body through sensors. Finally, the grid is fed from the antenna centre through a T-match impedance transformer [17] for fine tuning and control of the input impedance.

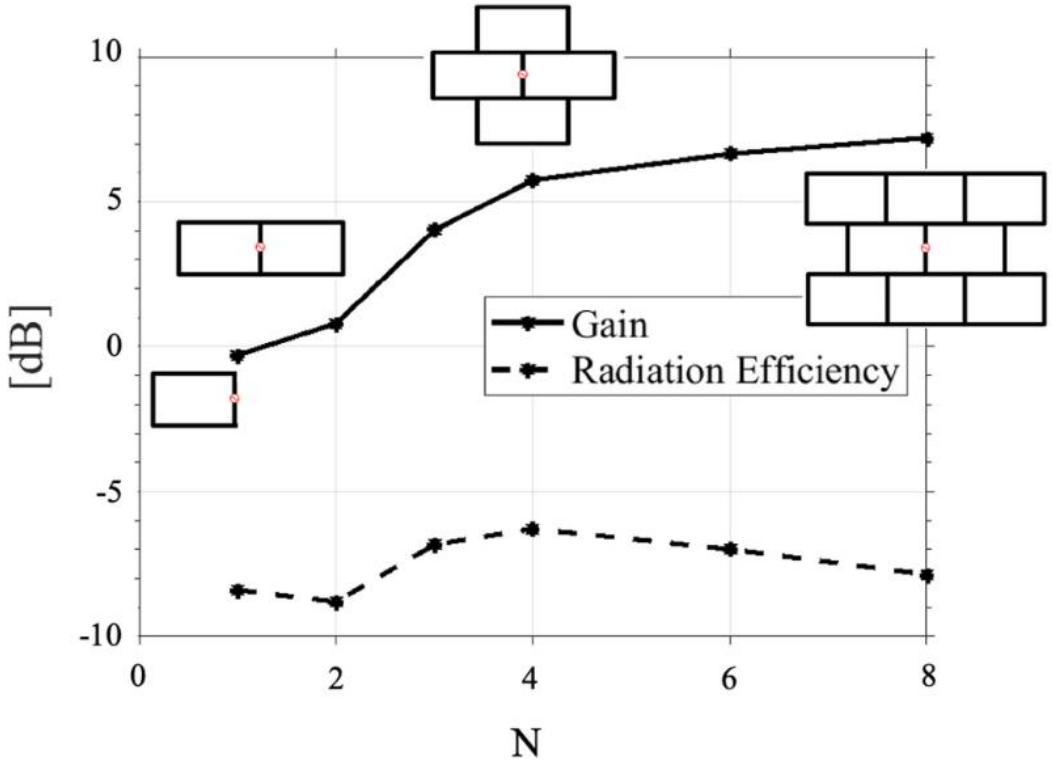

Fig. 2. Gain and radiation efficiency of the reference twin grid by varying the number of elements N. Efficiency is strongly affected by the radiation losses into the human body, caused by the attenuation of currents on the microstrip lines.

The radiation performance of the twin-grid array has been preliminary evaluated with the aim of finding the optimal size of both the driver and the reflector. Numerical simulations include a 150 × 150 × th mm^3 three-layer body phantom [6] [skin th = 1 mm, ε_r = 36.92, tan δ = 2.08, fat th = 3 mm, ε_r = 5.16, tan δ = 0.16, and muscle th = 31 mm, ε_r = 51.32, tan δ = 2.65 shown in Fig. 1(b)]. Analysis is carried out by varying the number of loop cells N and the width of the reflector conductor w_r. With attention focused on the radiation only, the grid is considered in transmitting mode and simply fed on the central vertical element without an impedance transformer, to be inserted later.

A. Optimal Number of Cells

The starting point is a resonant one-cell layout with parameters {h = 2 mm, s = 28.45 mm, l = 56.9 mm, w = 1 mm, w_r = 8 mm}, placed on a 2 mm thick ($\sim \lambda_{wg}/25$, $\lambda_{wg} \approx 56$ mm) biosilicone rubber slab. The gain increases with the number of elements N (see Fig. 2): moving from one cell (a single loop—with two vertical radiators) to eight cells (15 radiators), an improvement of about 8 dB is obtained. Similar to standard grids with continuous ground [18], the G(N) profile is not linear, since the increase in gain is limited by the attenuation of currents on the microstrip lines and by the poor control over the phase synchronization in case of large array. Furthermore, coherently with what was experienced with epidermal single layouts [6], the radiation performances of a skin array are the result of the balance between the array effect itself and power loss into the human body. The initial increase in the efficiency and gain is mostly due to the increase in the radiation resistance, which is

proportional to the number of vertical elements (6 dB of gain improvement by increasing four times the number of elements). Further enlargement of the grid produces more intense power dissipation on the conductors and within the surrounding tissues. The optimal efficiency arises for a grid array of four cells, with a maximum η = 35% (with corresponding gain $G_{\max}$ = 6 dBi); then, gain slowly improves, thanks to the more directive radiation pattern produced by a larger structure.

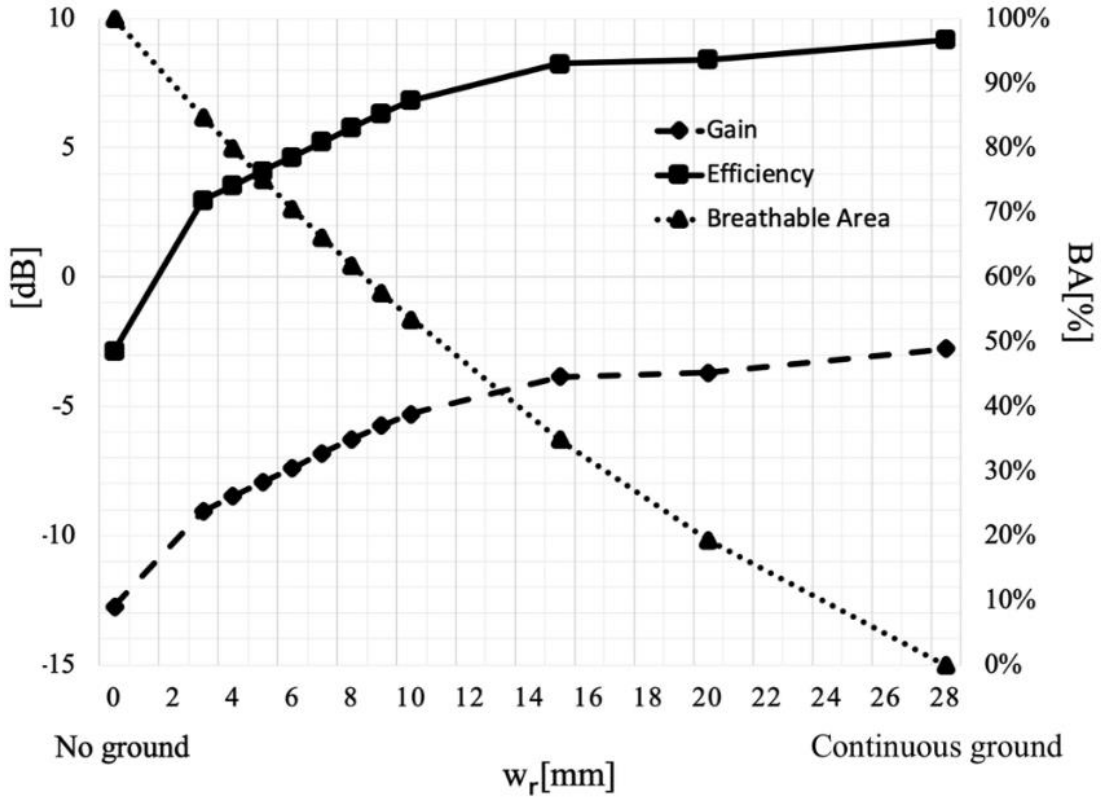

Fig. 3. Gain, radiation efficiency, and breathable area of the four-element twin grid by varying the width of the reflector trace wr .

B. Optimal Reflector Size

Gain and efficiency of the optimal four-element twin-grid array are shown in Fig. 3 by varying the trace width w_r of the reflecting grid. As w_r increases, the breathable area BA% = $[(l - w_r) \cdot (s - w_r)]/(l \cdot s)$ decreases with a better decoupling between body and array and consequently an improvement of both gain and efficiency. The size of the reflector affects the radiation performance especially in the early stages. A reduction of ∼ 15% of the breathable area (w_r = 3 mm) with respect to the ungrounded structure (BA = 100%) corresponds to an improvement in gain and efficiency of about 6 dB (more than double read distance with respect to the ungrounded structure). By reducing BA up to 50% (w_r = 10 mm), performance can be further improved, with $G_{\max} \approx 7$ dBi and η = −5 dB. An asymptotic profile is then observed. Overall, for w_r > 10 mm, there is only a modest improvement of the performances at the expenses of bulkiness of the device. Thus, a reasonable choice of the reflector parameter could be $8 \leq w_r \leq 10$ mm.

III. DESIGN OF A PROTOTYPE AND TESTING

A prototype of the four-element twin-grid array with w_r = 8 mm has been fabricated and experimentally characterized. Since backscattering transponders such as in the UHF band are not available yet 1 at 3.6 GHz, the grid has been matched to Zl = 50 Ω. The array is now fed through the T-match [see Fig. 4(a)], useful also for postproduction manual tuning to compensate for possible effects of human variability and prototyping uncertainties.

Starting from λ_{wg}, s and l have been slightly varied to obtain the proper pattern of current [see Fig. 4(b)] at the operating frequency f0 = 3.6 GHz, corresponding to seven dipoles radiating in phase. The resonant grid alternates series and parallel resonances, as shown in Fig. 5: by acting on the length of {a, b}, the input impedance Zin has been modified such to match Zl (Zin = 53.4 + 0.5 [Ω]). The final design parameters are listed in Table I. For other combinations of {a, b} parameters, inductive reactances, as required for matching typical RFID IC impedance, can be synthesized as well [17].

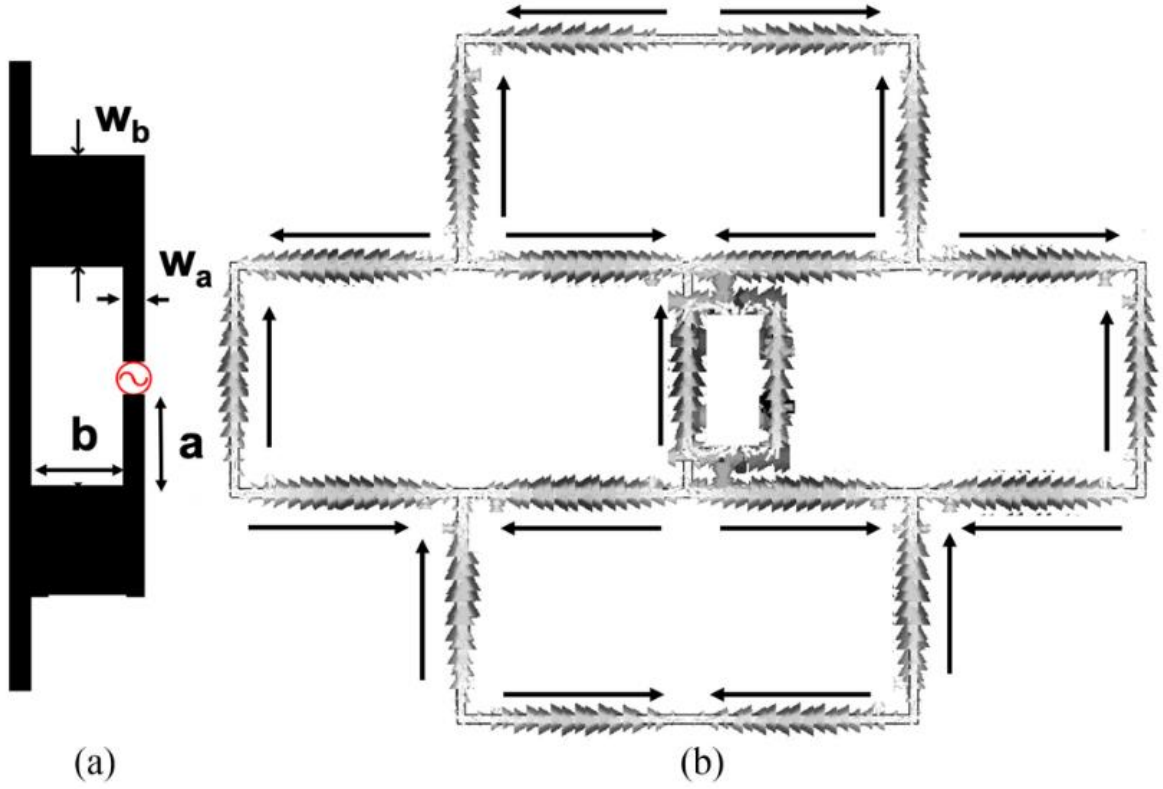

Fig. 4. (a) Detail of the feeding modality through a T-match transformer to finely control the input impedance of the grid array. (b) Pattern of current of the resonant four-element epidermal grid array with parameter in Table I.

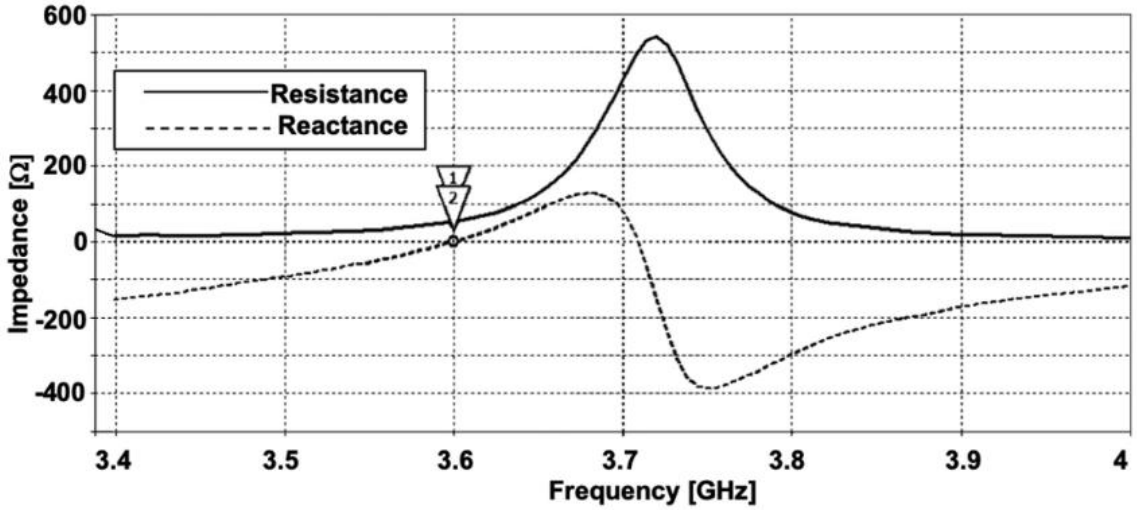

Fig. 5. Simulated input impedance Zin of the four-cell twin-grid array (parameters in Table I). Parallel and series resonances alternate; by acting on the shape factor of the T-match, the antenna can be matched to Zl = 50 Ω.

TABLE I
PARAMETERS OF THE REALIZED PROTOTYPES

	s	l	h	a	b	w_r	w	w_a	w_b
Twin-grids	28.45	56.9	2	10	8	8	1	1	4
Full Ground	28.25	56.5	2	8	6.8	28	1	1	5

The radiation pattern is shown in Fig. 6. A maximum broadside gain $G_{\max}$ = 6 dBi (BWV,−3dB = 54.6◦, BWH,−3dB = 34.5◦) and a radiation efficiency η = −5.5 dB are achieved. Under simplified hypothesis (free-space interaction, impedance matching, and polarization alignment), the maximum reading range can be derived from the Friis equation [3]. Since 5G-oriented electronics for backscattering radios are not yet available, it will be hereafter assumed that the powers radiated from the reader (EIRP = 3.2 W) and the sensitivities of current state-of-the-art UHF-RFID sensing-oriented components (P_{chip} = −15 dBm) could be achieved for 5G frequencies as well [6]. A maximum read distance of d = 4 m could hence be obtained. The grid has been fabricated by carving out adhesive copper (thickness 25 μm) by means of a two-axis cutter (Secabo S60). As a benchmark, the full-ground layout has also been fabricated and tested. The final prototype is shown in Fig. 7.

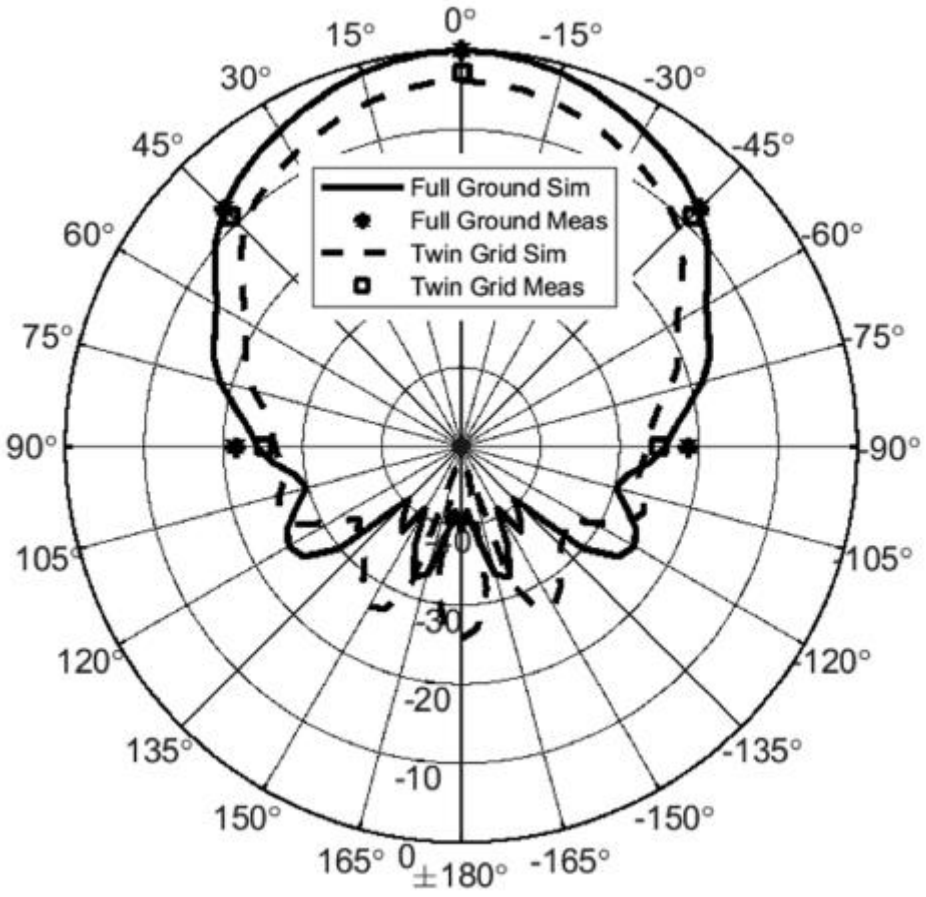

Fig. 6. Measured |S12|2 on the horizontal plane overlapped on simulated data. Data normalized with respect to the full ground maximum.

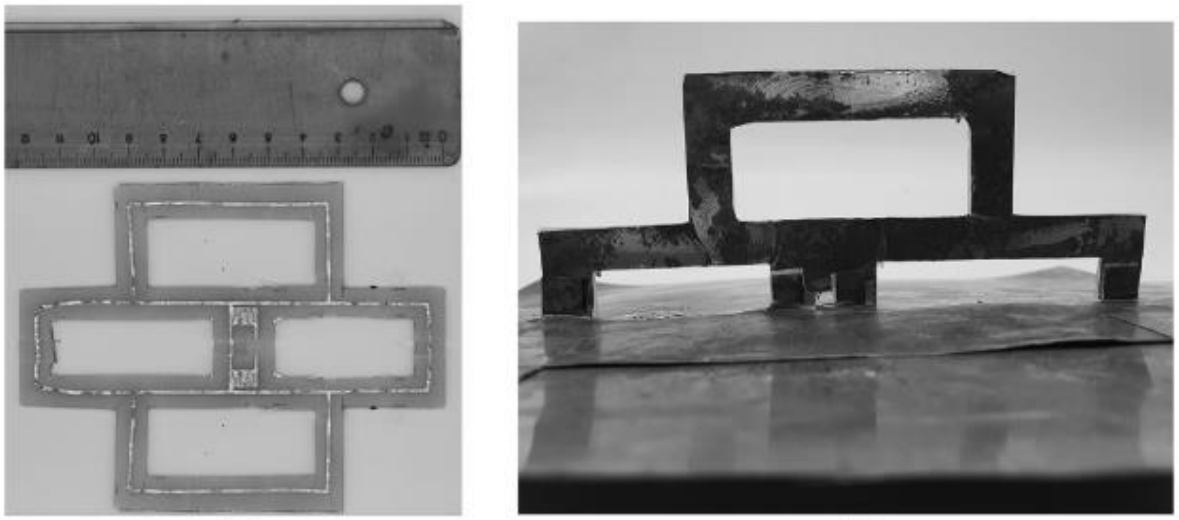

Fig. 7. Prototypes of the twin-grid array. (a) Front view and (b) back view of the measured half structure.

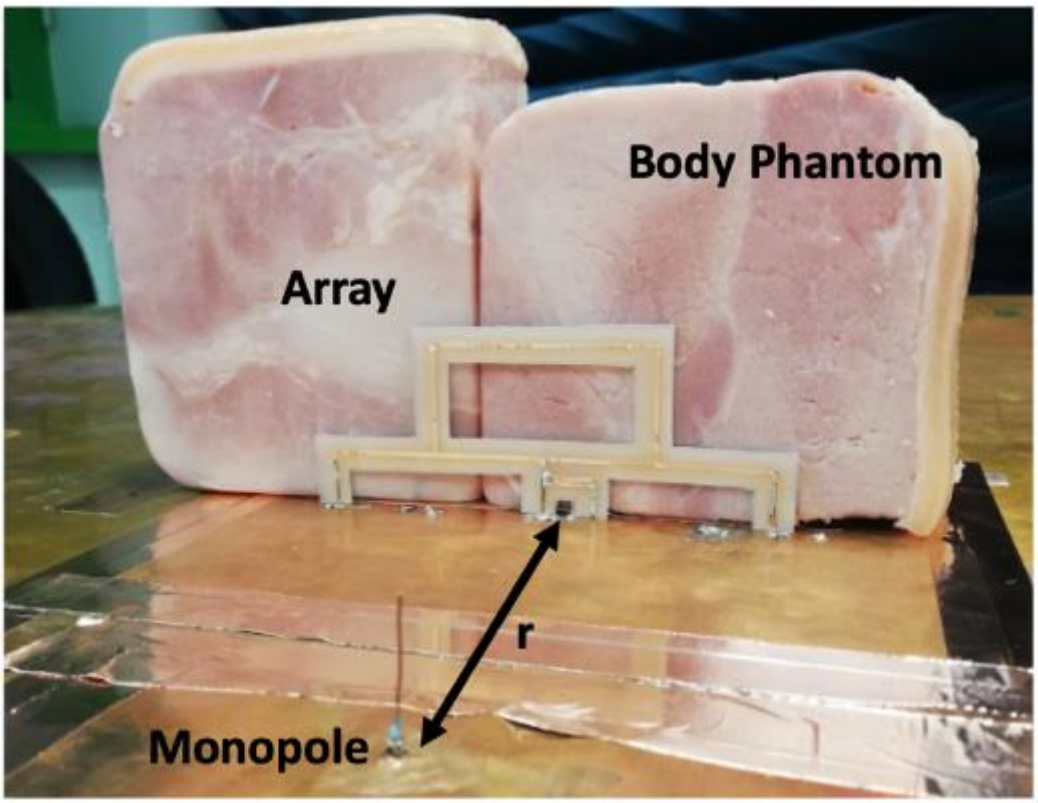

Fig. 8. Experimental setup for measuring the S-parameters of half-grid when attached onto a roasted pork phantom.

A. Measurements

Grid arrays were experimentally characterized by exploiting the image principle. A planar half-structure was vertically mounted on a large ground plane (size 1 m × 1 m, more than ten wavelengths from the radiating elements in each direction) and attached onto a cubic body phantom (roasted pork with estimated parameters ε_r = 40 and σ = 2 S/m [6]), as shown in Fig. 8. A l_m = 20 mm wire monopole probe placed at a distance r = 13 cm from the grid array was included to indirectly evaluate the radiation performances of the prototypes. The scattering parameters S were measured by a vector network analyser (HP 8517A). By assuming that the cables and the network analyser are perfectly matched, the radiation performances of the epidermal antenna can be retrieved by measuring the S12, since $|S12|^2 \propto$ G [16]. For corroboration, the entire system has been numerically evaluated as well.

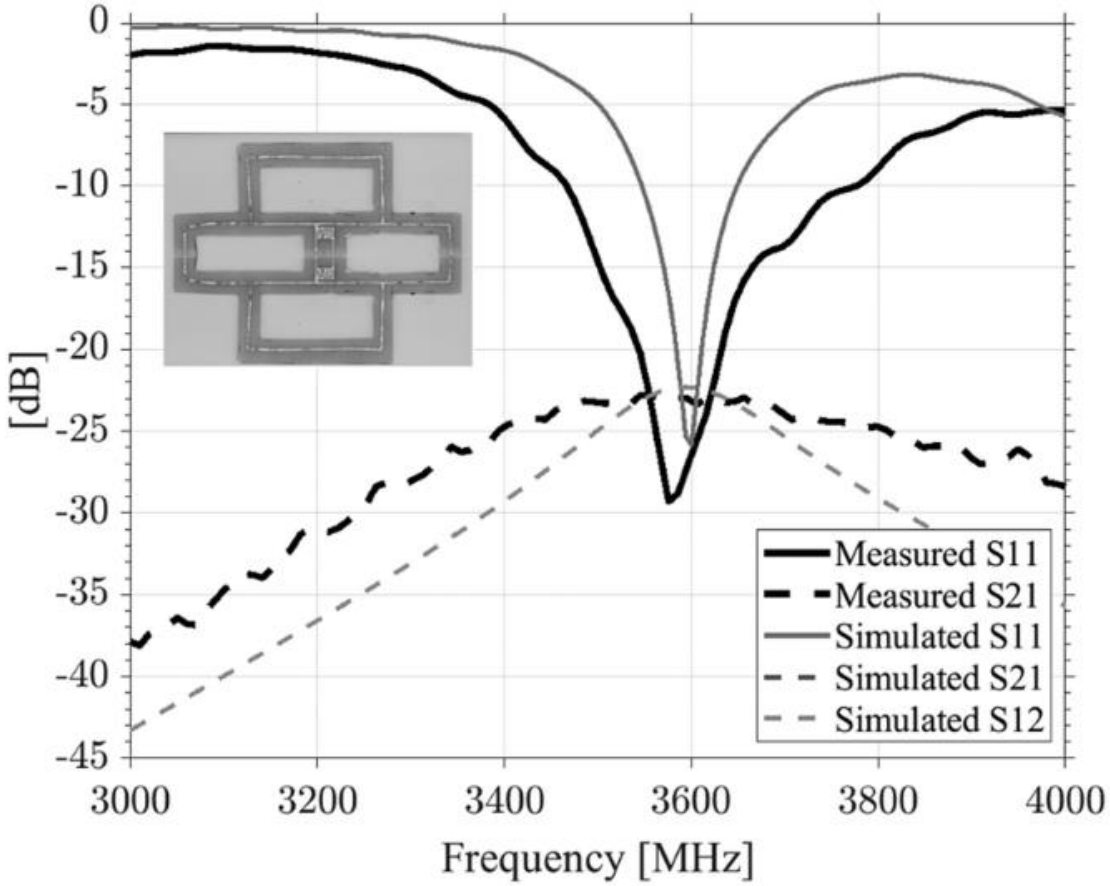

Fig. 9. Simulated and measured S-parameters of the half twin-grid array sourced by a test monopole.

Both antennas were slightly manually tuned at 3.6 GHz by acting on the T-match trace w_b to compensate for uncertainties in realization and phantom. Consequently, a good matching was obtained (see Fig. 9), in agreement with the simulations. Bandwidth BW−10dB = 8.6% is larger than the expected one, probably due to additional losses in the phantom, glue, and coaxial cables. The measured S12 of the structure with the grid reflector is approximately 3 dB lower than the one of the full ground layout, as visible in Fig. 6. By rotating the grid antenna with respect to the monopole probe, $|S12(\varphi)|^2$ has been evaluated also for different angles φ on the horizontal plane. Agreement with simulation is maintained. It is worth mentioning that this array configuration is body matched, i.e., it generates a broadside radiation only when it is placed on the skin. In the free space, instead, the reflector grid is ineffective, and a bidirectional pattern is produced.

IV. CONCLUSION

A soft and breathable grid array antenna has been simulated and fabricated for on-body epidermal applications at the 5G sub 6 GHz band. The array is suitable to be applied in different body regions such as abdomen, shoulder, and back. Promising results have been obtained in terms of impedance matching and gain. With respect to the single loop, a configuration with four cells offers a radiation gain 6 dB higher, corresponding to a doubling of the expected read distances. By considering the actual UHF RFID features (emitted power and IC sensitivities) valid in the S-band, read distances greater than 3 m are expected, even with a thin reflector. Such distances could be suitable to continuously track the vital signs of a user within a room, thus greatly extending the current performances of UHF epidermal systems.

REFERENCES

[1] D. H. Kim et al., “Epidermal electronics,” Science, vol. 333, no. 6044, pp. 838–843, 2011.

[2] S. Han et al., “Battery-free, wireless sensors for full-body pressure and temperature mapping,” Sci. Transl. Med., vol. 10, no. 435, 2018, Art. no. eaan4950.

[3] D. Dobkin, The RF in RFID, 4th ed. Burlington, MA, USA: Elsevier, 2012.

[4] S. Amendola, C. Occhiuzzi, and G. Marrocco, “More than wearable: Epidermal antennas for tracking and sensing,” in Electromagnetics of Body Area Networks: Antennas, Propagation, and RF Systems. Hoboken, NJ, USA: Wiley, 2016.

[5] N. F. M. Aun et al., “Revolutionizing wearables for 5G: 5G technologies: Recent developments and future perspectives for wearable devices and antennas,” IEEE Microw. Mag., vol. 18, no. 3, pp. 108–124, May 2017.

[6] F. Amato, C. Occhiuzzi, and G. Marrocco, “Epidermal backscattering antennas in the 5G framework: Performance and perspectives,” IEEE J.Radio Freq. Identif., vol. 4, no. 3, pp. 176–185, Sep. 2020.

[7] H. A. Damis, N. Khalid, R. Mirzavand, H. Chung, and P. Mousavi, “Investigation of epidermal loop antennas for biotelemetry IoT applications,” IEEE Access, vol. 6, pp. 15806–15815, 2018.

[8] S. Amendola and G. Marrocco, “Optimal performance of epidermal antennas for UHF radio frequency identification and sensing,” IEEE Trans. Antennas Propag., vol. 65, no. 2, pp. 473–481, Feb. 2017.

[9] P. S. Hall and Y. Hao, Eds., Antennas and Propagation for Body-Centric Wireless Communications, 1st ed. Norwood, MA, USA: Artech House, Aug. 2006.

[10] A. Pellegrini et al., “Antennas and propagation for body-centric wireless communications at millimeter-wave frequencies: A review,” IEEE Antennas Propag. Mag., vol. 55, no. 4, pp. 262–287, Aug. 2013.

[11] G. Gao, B. Hu, S. Wang, and C. Yang, “Wearable circular ring slot antenna with EBG structure for wireless body area network,” IEEE Antennas Wireless Propag. Lett., vol. 17, no. 3, pp. 434–437, Mar. 2018.

[12] E. Workman, I. Chang, and S. Noghanian, “Flexible textile antenna array,” in Proc. IEEE Int. Conf. Electro/Inf. Technol., 2015, pp. 569–574.

[13] C. Occhiuzzi and G. Marrocco, “Monolithic antenna array for epidermal 5G backscattering communications,” in Proc. 14th Eur. Conf. Antennas Propag., 2020, pp. 1–3.

[14] H. Nakano, T. Kawano, and J. Yamauchi, “Meander-line grid-array antenna,” Proc. Inst. Elect. Eng.—Microw., Antennas Propag., vol. 145, no. 4, pp. 309–312, Aug. 1998.

[15] M. Sun, Y. P. Zhang, Y. X. Guo, K. M. Chua, and L. L. Wai, “Integration of grid array antenna in chip package for highly integrated 60-GHz radios,” IEEE Antennas Wireless Propag. Lett., vol. 8, pp. 1364–1366, 2009.

[16] S. Orfanidis, Electromagnetic Waves and Antennas. New Brunswick, NJ, USA: Rutgers Univ. Press, Aug. 2010.

[17] G. Marrocco, “The art of UHF RFID antenna design: Impedance-matching and size-reduction techniques,” IEEE Antennas Propag. Mag., vol. 50, no. 1, pp. 66–79, Feb. 2008.

[18] B. Zhang and Y. P. Zhang, “Analysis and synthesis of millimeter-wave microstrip grid-array antennas,” IEEE Antennas Propag. Mag., vol. 53, no. 6, pp. 42–55, Dec. 2011.

[19] F. Amato, A. Di Carlofelice, C. Occhiuzzi, P. Tognolatti, and G. Marrocco, “S-band testbed for 5G epidermal RFIDs,” in Proc. URSI Gen. Assem. Sci. Symp., Rome, Italy, Aug. 29–Sep. 5, 2020, pp. 1–3.